Optics Letters

Carrier-envelope-phase stabilization via dual wavelength pumping

Marcus Seidel,[1,*] Jonathan Brons,[1] Fabian Lücking,[2] Vladimir Pervak,[2] Alexander Apolonski,[1,2] Thomas Udem,[1] and Oleg Pronin[1]

[1]Max-Planck-Institut für Quantenoptik, Hans-Kopfermann-Str. 1, D-85748 Garching, Germany
[2]Ludwig-Maximilians-Universität München, Am Coulombwall 1, D-85748 Garching, Germany
*Corresponding author: marcus.seidel@mpq.mpg.de

Received 5 January 2016; revised 4 March 2016; accepted 7 March 2016; posted 17 March 2016 (Doc. ID 255649); published 15 April 2016

A power-scalable concept for carrier-envelope-phase stabilization is presented. It takes advantage of simultaneous pumping of the zero- and first-phonon absorption line of Yb:YAG at 969 and 940 nm. The concept was implemented to lock the carrier-envelope-offset frequency of a 45 W average power Kerr-lens mode-locked thin-disk oscillator. The lock performance is compared to previous experiments where carrier-envelope-stabilization was realized by means of cavity loss modulation.

OCIS codes: (140.3425) Laser stabilization; (140.3480) Lasers, diode-pumped; (140.4050) Mode-locked lasers; (140.7090) Ultrafast lasers.

http://dx.doi.org/10.1364/OL.41.001853

Mode-locked thin-disk (TD) oscillators have experienced tremendous development during the past couple of years. Femtosecond (fs) pulse trains with average powers of more than 250 W were directly generated by such oscillators [1,2]. Extracavity compression resulted in pulse durations of less than three optical cycles [3,4] and peak powers of up to 140 MW [5]. Moreover, first experiments have been conducted to generate high harmonics at the full oscillator repetition rate [6]. However, the most exciting applications, such as XUV frequency comb spectroscopy [7] and attosecond pulse generation at MHz rates [8–10], require carrier-envelope-phase (CEP) stabilization of these high-power oscillators.

Since the first demonstration of CEP stabilization [11,12] several methods have been realized to reduce CEP noise. Usually, the amplitude-to-phase coupling in the gain or Kerr medium of the oscillator is exploited to control the carrier-envelope-offset frequency (f_{ceo}). In the majority of low-power oscillators (<10 W average power), the pump power is modulated. In diode-pumped oscillators and fiber lasers; this modulation is realized via controlling the pump diode current [13–15], while an acousto-optic modulator (AOM) is placed in the pump arm in the case of Ti:Sa oscillators [16]. Moreover, it has been shown that cavity loss modulation works as well to stabilize the CEP [17]. In fact, CEP stabilization at high average powers (>10 W) has only been demonstrated by means of intracavity loss modulation so-far [4]. In that case, an AOM was placed directly inside the oscillator. In the experiments presented here, the same oscillator was utilized but without the AOM or any other additional intracavity element that may cause thermal effects or adverse self-focusing. Instead, the gain of the active laser medium was modulated via dual-wavelength pumping. This demonstrates a fully power-scalable approach to CEP stabilization.

The experimental setup is sketched in Fig. 1. The Kerr-lens mode-locked (KLM) TD oscillator is described in detail in [18]. It delivers 250 fs pulses with 1.2 μJ energy at a 37.5 MHz repetition rate and 1030 nm central wavelength. About 20–25 W of average power were coupled into an 8 cm large mode area fiber (LMA 35). The pulses were subsequently compressed to a 20–25 fs duration by means of chirped mirrors [4]. About 400 mW of the short pulses were sent into an f-to-2f-interferometer. The input powers at the nonlinear fibers were adjusted with half-wave plates and

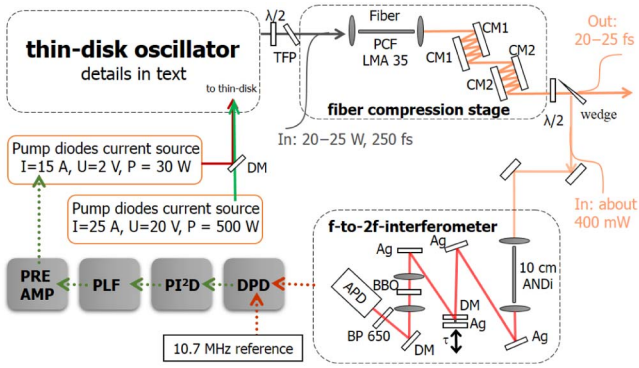

Fig. 1. Setup of the CEP stabilization scheme. Solid lines are optical, dotted lines electronic signals; $\lambda/2$, half-wave plate; TFP, thin film polarizer; CM, chirped mirror; Ag, silver mirror; DM, dichroic mirror; BP 650, band pass centered at 650 nm with $\Delta\lambda = 10$ nm, τ, delay stage to temporally overlap fundamental and second harmonic; APD, avalanche photo diode; DPD, digital phase detector; PI^{2}D, servo controller; PLF, phase lead filter; PREAMP, low noise preamplifier.

polarizers to maximize the beat note signal-to-noise ratio (SNR). While a fiber with anomalous dispersion was used in [4], an all-normal-dispersion fiber (ANDi, NKT NL-1050-NEG-1) was utilized in the presented experiments to generate the octave spanning continuum. The fiber exhibited a better stability during the time in which the PID controller settings were optimized (i.e., over about half an hour). A beat note could not be detected when the 250 fs pulses from the oscillator were directly launched into the ANDi fiber. Although full coherence of the octave-spanning continuum was computed even for 300 fs input pulses [19], polarization instabilities may have led to the loss of temporal coherence [20]. Contrary to [4], where a periodically poled crystal was used, second-harmonic generation was realized with a 1 mm thick BBO crystal. It could readily be tuned to double 1300 nm, which worked best for the continuum generated through the ANDi fiber. The beat note SNR was measured to be 35–40 dB (within 10 kHz resolution bandwidth).

To determine the feedback loop requirements, the free beat signal was sampled by a fast oscilloscope. The real signal was Hilbert-transformed to perform an analytic continuation to the complex plane and get access to the phase. Complex and real signal are related by [21]

$$\tilde{a}(t) = a(t) + i\mathcal{H}\{a(t)\}, \tag{1}$$

where $\mathcal{H}$ is the Hilbert-transform operator, $a(t)$ the real and $\tilde{a}(t)$ the complex beat signal. The carrier envelope offset frequency is then derived by

$$f_{\mathrm{ceo}}(t) = \frac{1}{2\pi}\frac{d}{dt}\Im\{\ln[\tilde{a}(t)]\}, \tag{2}$$

where $\Im$ denotes the imaginary part of the expression in braces. More details on the numerical beat note analysis are given in the appendix. In the experiment, the oscilloscope sampling rate was set to 25 megasamples per second. By virtue of the Nyquist–Shannon sampling theorem, instantaneous carrier envelope offset frequencies up to 12.5 MHz could hence be detected. By adjusting the pump current, the f_{ceo} was set to about 11 MHz. The spectral resolution was given by the measurement time of an oscilloscope trace. It was set to 0.5 s, resulting in a 2 Hz frequency spacing. The residual noise of the locked CEP was determined with this numerical method and a digital phase detector (DPD, [22]). The agreement was good, as the inset in Fig. 2 shows. This proves the accuracy of the numerical method. The integrated phase noise (IPN) at frequency f is calculated by

$$\mathrm{IPN}(f) = \left[\int_f^{f_{\max}} \mathrm{PSD}_\varphi(\nu)\mathrm{d}\nu\right]^{1/2}, \tag{3}$$

where PSD_φ is the power spectral density of the measured phase φ. It is computed by means of fast Fourier transforming the time-dependent signal. The upper integration boundary was usually set to $f_{\max} = 500$ kHz, where the phase error is already below the noise floor of the detection scheme.

The IPN of the free-running beat note is shown in Fig. 2. A phase noise of 100 mrad is accumulated after an observation time of 30 μs. This noise value shall be taken as reference because in many CEP sensitive time-domain applications a subradian residual noise is desired. Consequently, the feedback loop requires a bandwidth of at least 30 kHz. To implement this is challenging because: (i) the power supply of the pump diodes has to provide more than 400 W of electrical power and should also exhibit a flat modulation response. Furthermore, (ii) the low-pass filter function of the gain medium due to the ≈1 ms upper-state lifetime of the Yb ions has to be overcome.

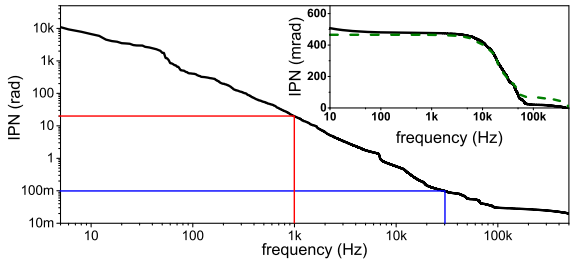

Fig. 2. IPN of the free-running beat note. The blue lines display the characteristic frequency where 100 mrad phase noise is accumulated. The red curve displays the characteristic frequency, which approximately corresponds to the upper state lifetime of the Yb^{3+} ions. The inset shows two consecutive measurements of the in-loop phase noise while feedback was applied to the pump diodes. The solid black line presents an analysis with the numerical method, the dashed green line with the DPD.

Challenge (i) was addressed by a dual-wavelength pumping scheme. The pump diodes operating at 940 nm are driven by a stable high-power supply (ILX lightwave LDX-36000). A second diode unit, radiating at 969 nm, is driven by a supply with less power but with the capability of broadband modulation (Thorlabs ITC4020). Both diode laser units pump the $^2F_{5/2}$–$^2F_{7/2}$ transition of the Yb^{3+} ions. Their radiation was combined by a homemade dichroic mirror before entering the TD head. The transfer function of the 969 nm pump diodes is depicted by the red lines in Fig. 3. A 90° phase lag is reached at about 60 kHz modulation frequency. The amplitude response is nearly flat up to this point. Therefore, the power supply proves to be suited for providing feedback over the targeted bandwidth. The standard deviation of the free-running beat note analyzed in Fig. 2 is about 350 kHz. This frequency shift is accomplished by a pump power change of 35 mW corresponding to 0.04% of the total pump power. Subsequently, the marginal intracavity power modulation needed for CEP stabilization does not affect the KLM stability.

The transfer function looked significantly different when the pump power modulation response of the TD oscillator was monitored with a fast photodiode. It is represented by the black lines in Fig. 3. In this case, a 90° phase lag is already present at frequencies higher than 10 kHz. Also, the amplitude

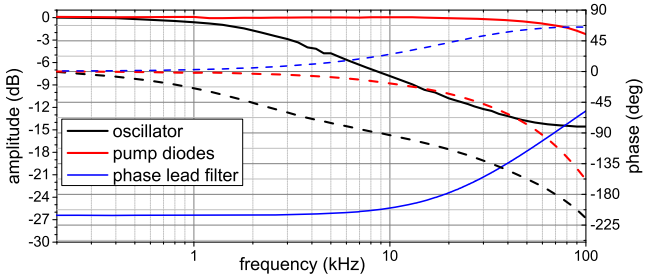

Fig. 3. Transfer functions of the 969 nm pump diodes power (red lines), the TD oscillator power (black lines), and the utilized PLF (blue lines). The solid lines display the amplitudes, and the dashed lines display the corresponding phases. The transfer functions of the PLF have been measured with a SRS SR780 network analyzer, the other transfer functions with an SRS SR830 lock-in amplifier.

response has dropped by 8 dB at that frequency. This intrinsic low-pass filtering, which presents challenge (ii), was counteracted by an electronic phase lead filter (PLF, blue lines Fig. 3) [13,15]. Due to the positive phase of the first-order high pass, the 90° phase lag is shifted to higher frequencies and the accessible bandwidth of the feedback loop is extended. Moreover, the slope of the PLF amplitude response is opposite that of the oscillator. The total attenuation of the feedback signal is compensated by an additional low-noise preamplifier (SRS SR560) which amplifies the signal by a 23 dB voltage gain over the whole bandwidth.

In order to minimize the residual CEP noise, the cutoff frequencies of the integral parts, the cut-on frequency of the derivative part and the proportional gain of the laser servo controller (Vescent Photonics D2-125) were varied. The in-loop phase noise could be reduced to 390 mrad (1 Hz–500 kHz) by setting the cutoff frequencies to 200 Hz and 5 kHz and the cut-on frequency to 20 kHz. The power spectral density of the detected beat signal phase and the IPN are shown in Fig. 4.

Contrary to the experiments presented in [4], no out-of-loop CEP noise measurements have been performed. Instead of presenting a CEP noise value, the in-loop phase error is compared to the previous experiments with the AOM. Since the locking electronics have not been changed, the relation between in-loop phase noise and the CEP noise are expected to be similar to [4]. A precise characterization does not give any additional insights into the stabilization concept, and hence was omitted.

There are two distinct spikes in the power spectral density. One is at 7 kHz and accounts for about 50 mrad phase noise. It is also visible in the free-running beat note noise and originates from the oscillator. This spike has not been observed in [4] and thus should be removable after an oscillator realignment. Although its exact origin is unknown, the possibility that the signature stems from the additional pump light at 969 nm can be excluded. The feature was also observed in the free-running beat note without the use of the second power supply. Another spike is at 44 kHz and accounts for an accumulated phase noise of about 125 mrad. This noise is inscribed by the phase-locked loop, which becomes resonant at this frequency due to the increasing phase lag. Most of the remaining noise is accumulated between these two spikes. The lock performance in this spectral region could certainly be improved, for instance, by a better design of the PLF. One approach was to measure the transfer function of the f_{ceo} and tailor the PLF to this function in order to get a flat response over the whole feedback bandwidth.

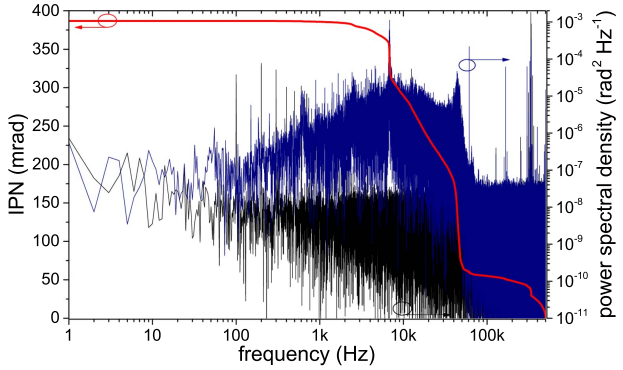

Fig. 4. Residual in-loop phase noise. The blue curve shows the power spectral density of the residual noise and the red curve the IPN from 500 kHz down to 1 Hz. The noise floor PSD is displayed in black.

The intracavity AOM loss modulation approach [4] shows that clearly lower CEP noise levels can be reached with the high power oscillator (180 mrad in-loop). The AOM intrinsically provides a very flat response up to hundreds of kHz and avoids the stated challenges by modulating the cavity losses and not the round trip gain. Nevertheless, the dual wavelength approach should also be capable of reaching sub-200 mrad CEP noise levels if the phase response is optimally shaped. The utilized power supply is specified with a 100% modulation depth without the loss of bandwidth at 225 W maximal electrical power. It is inferred that diodes of up to 100 W optical power can be driven with the supply. This is about 3 orders of magnitude more than the modulation amplitude required in the presented experiments. Subsequently, the concept is expected to be scalable to multiple kW of TD oscillator output power.

It is instructive to compare the noise accumulation of the free beat note in Fig. 2 to the transfer functions presented in [23]. The Yb:YAG TD oscillator mode-locked with a semiconductor saturable absorber mirror (SESAM) shows a strong resonance around 7 kHz and an abrupt phase behavior at this frequency, which was attributed to the saturable absorber. The combination of high average and peak power makes it difficult to operate the SESAM in the well-saturated regime. In particular, multiphoton absorption at the presence of several kW intracavity average power may lead to strong thermal lensing and rapid degradation. Consequently, SESAM mode-locking high-power TD oscillators appears to make CEP stabilization significantly more difficult than KLM, where the saturation behavior is determined through the interplay of the Kerr-lens with hard and soft apertures.

The presented concept can be generalized to the combination of a high power, highly stable signal with a lower power signal that can be modulated over a wide bandwidth. This combination was realized by means of optically combining radiation of 940 and 969 nm wavelength with a dichroic mirror. Both pump diodes and optical elements were readily available, making the presented setup favorable to implement the concept. Another approach was recently presented by Karlen *et al.* [24]. The low power signal modulated the stimulated emission rate of the Er:Yb:glass gain medium. This method could be transferred to TD oscillators if the pump optics would be coated appropriately. Moreover, an electronic combination of two power supplies is a possible approach if cross talk between the supplies can be avoided. Furthermore, the high power pump unit consists of multiple diode stacks, which are driven by a common power supply. Unfortunately, changing this was not offered by the diode unit supplier. Another method could make use of fiber combiners. A multimode fiber guides the pump light to the disk. Exchanging this fiber with one that combines the radiation of two sources could be a successful way to implement the stabilization scheme. Finally, it should be noted that the concept presented cannot only be used for CEP stabilization but also for intensity stabilization (i.e., "noise eating") of high-power oscillators.

In conclusion, a concept for CEP stabilizing high-power femtosecond oscillators has been introduced. The power scalable approach has led to a residual in-loop phase noise of 390 mrad (1 Hz–500 kHz) in a proof-of-principle

experiment with a 45 W average power KLM TD oscillator. The dual wavelength concept allows both highly stable pumping of the Yb:YAG gain medium and broadband modulation of the CEP. To reach a subradian residual in-loop noise performance, the low pass filtering behavior of the active laser medium was counteracted by a PLF. An optimized shaping of its transfer function promises a further reduction of the CEP jitter.

APPENDIX A: NUMERICAL BEAT NOTE ANALYSIS

Let $a(t)$ be the real beat signal taken with a fast oscilloscope. Its sampling rate is smaller than the repetition rate of the oscillator but larger than twice the maximal $f_{\mathrm{ceo}}(t)$ within the sampling time. Then $a(t)$ can be written as

$$a(t) = A(t) \cdot \cos(\varphi(t)) = A(t) \cdot \cos(\omega_{\mathrm{ceo}} t + \Delta\varphi(t)), \quad \textbf{(A1)}$$

where $A(t)$ and $\varphi(t)$ are the time-dependent amplitude and phase of the beat signal, $\omega_{\mathrm{ceo}} = 2\pi f_{\mathrm{ceo}}$, and $\Delta\varphi(t)$ is the time-dependent phase noise. The analytic continuation of the real signal to the complex domain is performed via Hilbert transformation as expressed in Eq. (1). The complex signal is

$$\tilde{a}(t) = A(t) \cdot \exp(i\omega_{\mathrm{ceo}} t + i\Delta\varphi(t)). \quad \textbf{(A2)}$$

Since an instantaneous frequency is defined by the change of phase in time, i.e.,

$$f(t) = \frac{1}{2\pi}\frac{d}{dt}\varphi(t), \quad \textbf{(A3)}$$

Eq. (2) follows.

For the sake of numerical processing, the following identities were used. On the one hand,

$$\frac{d}{dt}\ln(\tilde{a}(t)) = \frac{\frac{d}{dt}\tilde{a}(t)}{\tilde{a}(t)} = \frac{d}{dt}\ln(A(t)) + i\frac{d}{dt}\varphi(t). \quad \textbf{(A4)}$$

On the other hand,

$$\begin{aligned}\frac{\frac{d}{dt}\tilde{a}(t)}{\tilde{a}(t)} &= \frac{\Re\{\frac{d}{dt}\tilde{a}(t)\} + i\Im\{\frac{d}{dt}\tilde{a}(t)\}}{\Re\{\tilde{a}(t)\} + i\Im\{\tilde{a}(t)\}} \\ &= \frac{\left[\Re\{\tilde{a}(t)\}\Re\{\frac{d}{dt}\tilde{a}(t)\} + \Im\{\tilde{a}(t)\}\Im\{\frac{d}{dt}\tilde{a}(t)\}\right]}{|\tilde{a}(t)|^2} \\ &\quad + i\frac{\left[\Re\{\tilde{a}(t)\}\Im\{\frac{d}{dt}\tilde{a}(t)\} - \Im\{\tilde{a}(t)\}\Re\{\frac{d}{dt}\tilde{a}(t)\}\right]}{|\tilde{a}(t)|^2}.\end{aligned} \quad \textbf{(A5)}$$

Thus, it is found from Eqs. (A4) and (A5) that

$$\begin{aligned}\frac{d}{dt}\varphi(t) &= \frac{\left[\Re\{\tilde{a}(t)\}\Im\{\frac{d}{dt}\tilde{a}(t)\} - \Im\{\tilde{a}(t)\}\Re\{\frac{d}{dt}\tilde{a}(t)\}\right]}{|\tilde{a}(t)|^2} \\ &= \frac{a(t)\frac{d}{dt}[\mathcal{H}\{a(t)\}] - \mathcal{H}\{a(t)\}\frac{d}{dt}a(t)}{|\tilde{a}(t)|^2}.\end{aligned} \quad \textbf{(A6)}$$

This equation has been implemented in the numerical beat note analysis. The time derivatives were taken by means of fast Fourier transformation and multiplying the factor $i\omega$ in the frequency domain. Before transforming back into the time domain, the frequencies were bandpassed to reduce differentiation noise (from 10.5 to 12.5 MHz in the example shown in Fig. 2).

The advantages of this method are that Hilbert and Fourier transformation are relatively fast numeric algorithms. Contrary to short-time Fourier transformation, an instantaneous frequency can be determined for every sampling point. Moreover, through the normalization with $|\tilde{a}(t)|^2$ in Eq. (A6), the result is independent of amplitude fluctuations of the beat note signal and, in contrast to a DPD [22], the method does not only count zero crossings of the signal but utilizes all sampling points to compute the instantaneous f_{ceo}.

Funding. Munich-Centre of Advanced Photonics (MAP).

Acknowledgment. We thank Tadas Balciunas for the support in the PLF design, Christoph Gohle and Peter J. Delfyett for mathematical insights into the numerical beat note analysis, and Alexander Hartung for discussions on the ANDi fiber.

REFERENCES

1. C. J. Saraceno, F. Emaury, O. H. Heckl, C. R. E. Baer, M. Hoffmann, C. Schriber, M. Golling, T. Südmeyer, and U. Keller, Opt. Express **20**, 23535 (2012).
2. J. Brons, V. Pervak, E. Fedulova, D. Bauer, D. Sutter, V. Kalashnikov, A. Apolonskiy, O. Pronin, and F. Krausz, Opt. Lett. **39**, 6442 (2014).
3. K. F. Mak, M. Seidel, O. Pronin, M. H. Frosz, A. Abdolvand, V. Pervak, A. Apolonski, F. Krausz, J. C. Travers, and P. St.J. Russell, Opt. Lett. **40**, 1238 (2015).
4. O. Pronin, M. Seidel, F. Lücking, J. Brons, E. Fedulova, M. Trubetskov, V. Pervak, A. Apolonski, T. Udem, and F. Krausz, Nat. Commun. **6**, 6988 (2015).
5. J. Brons, V. Pervak, M. Seidel, D. Bauer, D. Sutter, O. Pronin, and F. Krausz, *Advanced Solid State Lasers (ASSL)* (Optical Society of America, 2015), paper ATh3A.1.
6. F. Emaury, A. Diebold, C. J. Saraceno, and U. Keller, Optica **2**, 980 (2015).
7. C. Gohle, T. Udem, M. Herrmann, J. Rauschenberger, R. Holzwarth, H. A. Schuessler, F. Krausz, and T. W. Hänsch, Nature **436**, 234 (2005).
8. M. Krebs, S. Hadrich, S. Demmler, J. Rothhardt, A. Zair, L. Chipperfield, J. Limpert, and A. Tünnermann, Nat. Photonics **7**, 555 (2013).
9. F. Krausz and M. I. Stockman, Nat. Photonics **8**, 205 (2014).
10. S. Hädrich, M. Krebs, A. Hoffmann, A. Klenke, J. Rothhardt, J. Limpert, and A. Tünnermann, Light Sci. Appl. **4**, e320 (2015).
11. D. J. Jones, S. A. Diddams, J. K. Ranka, A. Stentz, R. S. Windeler, J. L. Hall, and S. T. Cundiff, Science **288**, 635 (2000).
12. T. Udem, R. Holzwarth, and T. W. Hänsch, Nature **416**, 233 (2002).
13. J. McFerran, W. Swann, B. Washburn, and N. Newbury, Appl. Phys. B **86**, 219 (2007).
14. S. A. Meyer, J. A. Squier, and S. A. Diddams, Eur. Phys. J. D **48**, 19 (2008).
15. T. Balčiūnas, O. D. Mücke, P. Mišeikis, G. Andriukaitis, A. Pugžlys, L. Giniūnas, R. Danielius, R. Holzwarth, and A. Baltuška, Opt. Lett. **36**, 3242 (2011).
16. A. Poppe, R. Holzwarth, A. Apolonski, G. Tempea, C. Spielmann, T. Hänsch, and F. Krausz, Appl. Phys. B **72**, 373 (2001).
17. C.-C. Lee, C. Mohr, J. Bethge, S. Suzuki, M. E. Fermann, I. Hartl, and T. R. Schibli, Opt. Lett. **37**, 3084 (2012).
18. O. Pronin, J. Brons, C. Grasse, V. Pervak, G. Boehm, M.-C. Amann, V. L. Kalashnikov, A. Apolonski, and F. Krausz, Opt. Lett. **36**, 4746 (2011).
19. A. M. Heidt, J. Opt. Soc. Am. B **27**, 550 (2010).
20. Y. Liu, Y. Zhao, J. Lyngso, S. You, W. Wilson, H. Tu, and S. Boppart, J. Lightwave Technol. **33**, 1814 (2015).
21. J.-C. Diels and W. Rudolph, *Ultrashort Laser Pulse Phenomena*, 2nd ed., J.-C. D. Rudolph, ed. (Academic, 2006), pp. 1–60.
22. M. Prevedelli, T. Freegarde, and T. Hänsch, Appl. Phys. B **60**, S241 (1995).
23. F. Emaury, A. Diebold, A. Klenner, C. J. Saraceno, S. Schilt, T. Südmeyer, and U. Keller, Opt. Express **23**, 21836 (2015).
24. L. Karlen, G. Buchs, E. Portuondo-Campa, and S. Lecomte, Opt. Lett. **41**, 376 (2016).